

Constraining the Contribution of Galaxies and Active Galactic Nuclei to Cosmic Reionization

Shintaro Yoshiura^{1*}, Kenji Hasegawa², Kiyotomo Ichiki^{2,3}, Hiroyuki Tashiro², Hayato Shimabukuro^{1,2}, Keitaro Takahashi¹

¹*Department of Physics, Kumamoto University, Kumamoto, Japan*

²*Department of Physics, Nagoya University, Aichi, Japan*

³*Kobayashi-Maskawa Institute for the Origin of Particles and the Universe, Nagoya University Nagoya, 464-8602, Japan*

Accepted XXX. Received YYY; in original form ZZZ

ABSTRACT

Understanding the detailed process of cosmic reionization is one of the remaining problems in astrophysics and cosmology. Here we construct a model of cosmic reionization that includes contributions from high- z galaxies and active galactic nuclei (AGNs), and calculate the time evolutions of HI/HeII fractions of the universe. To keep the model to be general and realistic, we vary the escape fraction of ionizing photons, f_{esc} , and the faint-end slope of the AGN luminosity function at high redshifts, α_{hz} , within the constraints from the observed cosmic star formation history and the observed bright-end UV luminosity functions at $z \leq 6$. Additionally, we model the spectral energy distribution (SED) which depends on the Eddington ratio and the black-hole mass. By comparing the models with the observed HI/HeII fractions and the optical depth for Thomson scattering from Planck, we find that $\alpha_{\text{hz}} > -1.5$ and $f_{\text{esc}} < 0.15$ should be satisfied. Our result suggests that an AGN-dominated model with AGN abundance as large as the estimation of recent observation by Giallongo et al. is allowed only if the contribution from high- z galaxies is almost negligible, while a galaxy-dominant model is also allowed.

Key words: cosmology; dark ages, reionization, first stars

1 INTRODUCTION

It is generally believed that the Universe became neutral at $z \approx 1100$ (cosmic recombination) and was gradually ionized again by ionizing sources formed following cosmic recombination. The time evolution of this global transition called cosmic reionization has been widely explored. One of observational approaches to estimate neutral fractions at high redshifts is to measure absorption features imprinted on high- z quasar (QSO) spectra. The HI Lyman- α ($\text{Ly}\alpha$) absorption lines imprinted on QSOs spectra have indicated that hydrogen was almost reionized by $z \sim 6$ (Fan et al. 2006). Similar observations measuring HeII absorption lines have also shown that helium reionization was mostly completed by $z \approx 3$ (Becker et al. 2011; Worseck et al. 2014; Syphers & Shull 2014). Observing the redshift evolution of $\text{Ly}\alpha$ luminosity function ($\text{Ly}\alpha$ LF) can also provide valuable information on neutral hydrogen fractions during the epoch of reionization (EoR), because the detectability of $\text{Ly}\alpha$ radiation is very sensitive to the amount of neutral hydrogen. Recent observations for $z \geq 5.7$ $\text{Ly}\alpha$ emitters (LAEs)

have shown that the number density of LAEs decreases with redshift (Ota et al. 2010; Hu et al. 2010; Ouchi et al. 2010; Kashikawa et al. 2011; Konno et al. 2014). This fact implies that the neutral hydrogen fraction increases from $z \sim 6$ to $z \sim 7$. Furthermore, the measurements of the Cosmic Microwave Background (CMB) optical depth to Thomson scattering have imposed an additional constraint on the reionization history. The most recent observation by Planck has shown that the optical depth τ_e is 0.066 ± 0.016 which corresponds to an instantaneous reionization redshift of $z_r = 8.5 \pm 0.9$ (Planck Collaboration et al. 2016).

Despite the advancing understanding on the history of cosmic reionization, there is no crucial observation for the type of ionizing sources which was responsible for cosmic reionization. Revealing the type of ionizing sources is also important for understanding the process of reionization, since the mean free path of ionizing photons is essential for the reionization evolution.

High- z galaxies are thought to be plausible candidates for the ionizing sources, since a number of galaxies have already discovered at $z > 6$ (Ouchi et al. 2009; Oesch et al. 2014; Bouwens et al. 2015). In addition, some of recent observations have presented that the faint-end slopes of ul-

* E-mail: 161d9002@st.kumamoto-u.ac.jp

traviolet luminosity functions (UVLFs) during the EoR are steep and extended down to an absolute UV magnitude of $M_{UV} \sim -16$ (Atek et al. 2015; Ishigaki et al. 2015). These facts strengthen the possibility that the high- z galaxies were main ionizing sources of reionization. Robertson et al. (2015) have indeed shown that the Thomson scattering optical depth and HI fractions inferred from the QSO spectra and LAEs observations can be simultaneously achieved solely by high- z galaxies if the escape fraction of ionizing photons from the galaxies (f_{esc}) is as high as ~ 0.2 . However the escape fraction is highly uncertain.

At relatively low redshifts $z \sim 3$, Lyman continuum (LyC) photons from galaxies have directly been detected, and the escape fractions have been evaluated as $f_{\text{esc}} \sim 0.01 - 0.1$ (Steidel et al. 2001; Iwata et al. 2009), although some of the LyC emitters may be low- z contaminants (Siana et al. 2015). In contrast to galaxies at low redshifts, no ionizing photons from galaxies at the EoR has been detected due to strong attenuation by the intergalactic matter (IGM). However, Dunlop et al. (2013) have claimed that spectral energy distributions (SEDs) of high- z galaxies imply the escape fraction of $f_{\text{esc}} \approx 0.1 - 0.2$ with some assumptions. The escape fraction also has been assessed by numerical simulations (e.g. Gnedin et al. 2008; Razoumov & Sommer-Larsen 2010; Yajima et al. 2011; Paardekooper et al. 2014; Wise et al. 2014; Kimm & Cen 2014). Although most of the simulations show a similar trend, i.e. the escape fraction decreases with the mass of the galaxy, there is variance with ~ 1 -2 orders of magnitude among the simulation results. Thus, there is as yet no consensus on the value of the escape fraction, and this fact leads to the significant uncertainty of the contribution of high- z galaxies to cosmic reionization.

Active galactic nuclei (AGNs) are also expected to have been another type of ionizing sources. Since photons with energies above 54.4eV are required for doubly ionizing helium, AGNs are the most promising ionizing sources at the epoch when helium in the IGM is fully ionized, i.e. $z \sim 3$ (Becker et al. 2011; Worseck et al. 2014). However, it was traditionally believed that the contribution of AGNs to reionization is less important because of a rapid decrease in their abundance at $z > 3$ (Masters et al. 2012; Ueda et al. 2014). Very recently Giallongo et al. (2015) have found faint AGNs at $z \sim 4$ -6. This suggests that the contribution of AGNs to reionization could increase by orders of magnitude. Although it is still under debate, the contribution of AGNs might overcome that of galaxies if this claim was valid beyond $z \approx 6$. Unfortunately, while there is currently no direct observation for faint AGNs at $z > 6$, the contribution of AGNs could be imprinted on HI 21cm-line signal (Baek et al. 2010). Hence the Square Kilometer Array (SKA) and its pathfinders will tell us the information on the abundance of AGNs at $z > 6$.

Madau & Haardt (2015) (hereafter MH15) have calculated reionization history, extrapolating the evolution of AGN abundance reported by Giallongo et al. (2015) up to $z = 13$ and neglecting the contribution of galaxies. As a result, they have found that the ‘‘AGN-dominant scenario’’ can satisfy the observed HI/HeII fractions and Thomson scattering optical depth simultaneously. However, as described above, if f_{esc} is high, the additional contribution of galaxies would result in the overproduction of ionized

hydrogen and electron at $z > 6$. Hao et al. (2015) have also performed calculations including both of the galaxies and (faint-)AGNs, and found that their model is consistent with the EoR measurements, the Thomson scattering optical depth and helium reionization. However, they have neglected redshifted high energy photons which effectively ionize the IGM at lower redshifts, in particular, helium reionization. Mitra et al. (2016) have also investigated contribution of AGNs to reionization history by using their semi-analytic reionization model. They have pointed out that their high AGN emissivity model can reionize HI. Their model also leads to more rapid evolution of Lyman limit systems than in observations, while the reionization evolution by the combination of lower AGN emissivity and galaxies with the escape fraction of $\sim 10\%$ shows good agreement with the observation results. Khaire et al. (2016) have numerically shown that abundant faint AGNs or f_{esc} rising with redshift is required for explaining a constant photoionization rate at $3 < z < 5$ reported by observations. Very recently, Ricci et al. (2016) indicated excluding an AGN dominant scenario by X-ray selected AGN samples. They argued the contribution of AGNs at $z = 6$ is less than 30%.

It is well-known that the shape of SED controls the efficiency of the ionization and heating processes of the IGM. Therefore, the shape of SED plays an important role in the calculation for the EoR. However, in all of the recent studies, SEDs of AGNs have been assumed to be simple power-law spectra, in contrast to the theoretical prediction that the SED depends on the central black hole mass M_{BH} and the Eddington ratio $\gamma_{\text{Edd}} \equiv L/L_{\text{Edd}}$ where L_{Edd} is the Eddington luminosity (e.g. Kawaguchi et al. 2001). The contribution of AGNs to reionization cannot be qualitatively evaluated unless the SED shape of AGNs is considered appropriately.

In this work, we aim to constrain the contribution of galaxies and AGNs to cosmic reionization. For the purpose, we firstly build a model of the redshift evolution of the AGN emissivity in which the redshift evolution of the AGN LF and SED depending on the both of M_{BH} and λ_{Edd} are considered. Then, using the model, we compute H/He reionization histories with different parameter sets of f_{esc} and AGN abundance. Finally, we search possible contribution of galaxies and AGNs to reionization from the comparison between the computed reionization histories and observations.

The structure of this paper is as follows. In section 2, we describe the method for computing the hydrogen and helium reionization histories. In section 3, we show our numerical results and compare them to observed HI/HeII fractions. We discuss the implication of our results and comment on the model dependence in section 4. Finally the summary will be given in section 5. Throughout this paper, we assume Λ CDM cosmology with $(\Omega_{\text{m}}, \Omega_{\Lambda}, \Omega_{\text{b}}, H_0) = (0.308, 0.692, 0.02237, 67.80 \text{ km s}^{-1} \text{ Mpc}^{-1})$ (Planck Collaboration et al. 2015).

2 METHODOLOGY

The evolution of the ionization fraction f_i (for species $i = \text{HII}, \text{HeII}, \text{HeIII}$) can be written as

$$\frac{df_{\text{HII}}}{dt} = \Gamma_{\text{HI}} - \alpha_{\text{B,HII}} C n_e (1+z)^3 f_{\text{HII}}, \quad (1)$$

$$\begin{aligned} \frac{df_{\text{HeII}}}{dt} &= \Gamma_{\text{HeI}} - \Gamma_{\text{HeII}} \\ &- C n_e (1+z)^3 (\alpha_{\text{B,HeII}} f_{\text{HeII}} - \alpha_{\text{B,HeIII}} f_{\text{HeIII}}) \end{aligned} \quad (2)$$

$$\frac{df_{\text{HeIII}}}{dt} = \Gamma_{\text{HeII}} - \alpha_{\text{B,HeIII}} C n_e (1+z)^3 f_{\text{HeIII}}, \quad (3)$$

where $\alpha_{\text{B},i}$ is the case B recombination coefficient for each species, n_{H} , n_{He} , and n_e are the comoving number densities for hydrogen, helium, and electron, respectively. Here C is the clumping factor of the IGM and is set to be $C = 3$ as consistent with results from hydrodynamics simulations which take into account photo-heating of the IGM (Pawlik et al. 2009; Raicević & Theuns 2011). In this paper, the ionization rate for each species, Γ_i is decomposed into two components as $\Gamma_i = \Gamma_{*,i} + \Gamma_{\text{AGN},i}$, where $\Gamma_{*,i}$ is for photons from star forming galaxies and $\Gamma_{\text{AGN},i}$ for photons from AGNs. We will describe how we consider each contribution in the following sections.

Ionizing photons emitted by stars and AGNs also heat up the IGM. The IGM temperature is one of the important factors to describe the state of the IGM gas. The evolution of the IGM temperature T_e can be described as

$$\frac{dT_e}{dt} = \frac{2}{3} \frac{\mu}{k_{\text{B}} n_{\text{B}}} \left(\sum_i \epsilon_{\text{heat},i} - \epsilon_{\text{cool}} \right) - 2HT_e - \mu T_e \frac{d\mu^{-1}}{dt}, \quad (4)$$

where H is the Hubble parameter, k_{B} is the Boltzmann constant, μ is the mean molecular weight, n_{B} is the proper baryon number density, and ϵ_{cool} is the IGM cooling rate. We take into account the IGM cooling processes summarized in the appendix of Fukugita & Kawasaki (1994). In Eq. (4), $\epsilon_{\text{heat},i}$ describes the heating rate for each species i . We also decompose the heating rate to two components: from star forming galaxies, $\epsilon_{*,i}$, and from AGNs, $\epsilon_{\text{AGN},i}$, as Γ_i in the case of calculations of the ionization fraction.

When we solve Eqs. (1)-(4), we employ some artificial treatments to bypass some numerical inconveniences. As described later, we assume that all ionizing photons from star-forming galaxies are consumed to ionize the local IGM. Due to this treatment, f_{HII} can exceed 1.0 and f_{HI} essentially becomes zero. Unfortunately, this unrealistic behavior results in numerical oscillations of f_{HI} and f_{HII} . In order to avoid the unrealistic behavior we set the lower limit of neutral hydrogen fraction as $f_{\text{HII},1} = 10^{-4}$. However this artificial limit leads to the continual heating of the IGM. Thus we also set the upper limit of the temperature as $T_{e,u} = 20,000\text{K}$.

2.1 Ionizing photons from stars

Star forming galaxies are considered as main sources of ionizing photons. In a star forming galaxy, huge amount of UV photons are produced from stars. Some of these photons can escape from the galaxy and ionize the surrounding IGM.

To evaluate the ionization rates for star forming galaxies, $\Gamma_{*,i}$, we need to know the value of the escape fraction f_{esc} . However f_{esc} is highly uncertain as described in §1. Therefore, we take f_{esc} as a free parameter in our model.

Since f_{esc} controls the contribution of high- z galaxies to the cosmic reionization process, we obtain the constraint on f_{esc} from the comparison with observational data of the EoR. Using f_{esc} , we assume that the proper number density of photons emitted per unit time from star forming galaxies at a redshift z is proportional to the star formation rate density (SFRD),

$$\dot{n}_{*\nu} = (1+z)^3 f_{\text{esc}} \dot{\rho}_* \gamma_\nu, \quad (5)$$

where $\dot{\rho}_*$ is the comoving SFRD for which we adopt the fitting formula by Madau & Dickinson (2014),

$$\dot{\rho}_*(z) = 0.015 \frac{(1+z)^{2.7}}{1 + [(1+z)/2.9]^{5.6}} [\text{M}_\odot \text{yr}^{-1} \text{Mpc}^{-3}]. \quad (6)$$

In Eq. (5), γ_ν is the intrinsic number of photons produced by stars per solar mass at a frequency ν . For γ_ν , we use the correspondent formula in Choudhury & Ferrara (2005) that is derived by a population synthesis calculation,

$$\int_{\nu_1}^{\nu_2} d\nu \gamma_\nu = \begin{cases} 5.43 \times 10^{60} / \text{M}_\odot, & (\nu_1, \nu_2) = (\nu_{\text{HI}}, \nu_{\text{HeI}}), \\ 2.61 \times 10^{60} / \text{M}_\odot, & (\nu_1, \nu_2) = (\nu_{\text{HeI}}, \nu_{\text{HeII}}), \\ 0.01 \times 10^{60} / \text{M}_\odot, & (\nu_1, \nu_2) = (\nu_{\text{HeII}}, \nu_{\text{max},*}). \end{cases} \quad (7)$$

where $\nu_{\text{max},*}$ is the upper limit of the frequency we consider in this paper and is set to $h_{\text{p}} \nu_{\text{max},*} = 100 \text{eV}$. Here h_{p} is the Planck constant.

As mentioned above, the ionizing photons from star forming galaxies are in the UV range. Since UV photons have short mean free paths, they are consumed to ionize a local region of the IGM. This means that all photons from star forming galaxies can be assumed to contribute to ionize the local IGM. To calculate $\Gamma_{*,i}$ with this assumption, it is necessary to evaluate how much extent of photons from star forming galaxies is consumed for the ionization of the i -th species. The absorption rate of photons for each ionization is different. Therefore, the relative number of photons consumed for the ionization of the i -th species has to be proportional to the relative opacity of the corresponding species (e.g. Eqs. A5-A7 in Susa 2006). Taking into account the frequency dependence of the ionization cross sections for hydrogen and helium, we can write the ionization rate (proper ionizing photon number density per unit time) for the i -th species as

$$\Gamma_{*,i} = \frac{1}{(1+z)^3} \int_{\nu_i}^{\infty} d\nu \frac{f_i \sigma_i \dot{n}_{*\nu}}{n_{\text{HI}} \sigma_{\text{HI}} + n_{\text{HeI}} \sigma_{\text{HeI}} + n_{\text{HeII}} \sigma_{\text{HeII}}}, \quad (8)$$

where σ_i is the cross section for the i -th species and ν_i is the Lyman limit frequency of the i -th species, i.e. $h_{\text{p}} \nu_{\text{HI}} = 13.6 \text{eV}$, $h_{\text{p}} \nu_{\text{HeI}} = 24.5 \text{eV}$, and $h_{\text{p}} \nu_{\text{HeII}} = 54.4 \text{eV}$. In Eq. (8), n_j represents n_{H} for $i = \text{HI}$ and n_{He} for $i = \text{HeI}$ and HeII .

Next, we consider the heating rate due to UV radiation from star forming galaxies $\epsilon_{*,i}$. When a photon with a frequency ν ionizes a particle of the i -th species, the energy $h_{\text{p}}(\nu - \nu_i)$ contributes to heat the IGM gas. Thus, the heating rate $\epsilon_{*,i}$ for the i -th species is given by

$$\epsilon_{*,i} = \int_{\nu_i}^{\infty} d\nu \frac{n_i \sigma_i h_{\text{p}} (\nu - \nu_i) \dot{n}_{*\nu}}{n_{\text{HI}} \sigma_{\text{HI}} + n_{\text{HeI}} \sigma_{\text{HeI}} + n_{\text{HeII}} \sigma_{\text{HeII}}}. \quad (9)$$

As shown by Eq. (7), we only know the integrated γ_ν . Therefore, we perform the integration in Eqs. (8) and (9) by using the cross sections averaged over each frequency range.

2.2 Ionizing photons from AGNs

UV/X-ray photons from AGNs are also important in the reionization process of the IGM in the early Universe. X-ray photons have much larger mean free paths than UV photons and can ionize and heat up the IGM at cosmological distances. Therefore, to evaluate the ionization and heating rates at a redshift z , we need to take into account X-ray photons coming from AGNs at redshifts higher than z . Then, the ionization and heating rates are respectively given by,

$$\Gamma_{\text{AGN},i}(z) = \int_{\nu_i}^{\nu_{\text{max,AGN}}} \frac{d\nu}{h\nu} f_i \sigma_i (1+z)^3 F(z, \nu), \quad (10)$$

and

$$\epsilon_{\text{AGN},i}(z) = \int_{\nu_i}^{\nu_{\text{max,AGN}}} \frac{d\nu}{h\nu} \sigma_i(\nu) n_i h\nu (\nu - \nu_i) (1+z)^3 F(z, \nu). \quad (11)$$

where $F(z, \nu)$ represents the energy flux from AGNs at redshifts higher than z at a frequency ν . The upper bound of the integration, $\nu_{\text{max,AGN}}$, is set to be 2.4×10^{20} Hz which corresponds to the energy of 10^3 keV. The energy flux at z is calculated as

$$F(z, \nu) = \int_z dz' \epsilon_c(z', \nu') \frac{c(1+z)^2}{H} \exp(-\tau_X(z, z', \nu')), \quad (12)$$

where c is the speed of light and $\nu' = \nu(1+z)/(1+z')$. Here, $\epsilon_c(z, \nu)$ is the comoving emissivity at a redshift z and a frequency ν . As described in § 1, previous studies focusing on the contribution of AGNs to reionization (e.g. Madau & Haardt 2015; Hao et al. 2015; Mitra et al. 2016; Khaire et al. 2016) have assumed power-law spectra and the evolution of ϵ_c itself. They play important roles in the EoR process and depends on the evolution of AGNs. Therefore, we take into account the evolution of AGN LF and the SED depending on M_{BH} and λ_{Edd} to elucidate the AGN contribution at the EoR in more detail.

Using the SED L_ν and UVLF $\Phi(z, M_{\text{UV}})$ of AGNs, where M_{UV} is the absolute magnitude at the wavelength of 1450 Å, we can write $\epsilon_c(z, \nu)$ as

$$\epsilon_c(z, \nu) = \int_{M_{\text{UV}}^{\text{min}}}^{M_{\text{UV}}^{\text{max}}} L_\nu(M_{\text{UV}}) \Phi(z, M_{\text{UV}}) dM_{\text{UV}}. \quad (13)$$

The upper bound of the integration is fixed to be $M_{\text{UV}}^{\text{max}} = -34$, while the lower bound is set to $M_{\text{UV}}^{\text{min}} = -18$ as a fiducial value. The SED L_ν is a function of M_{UV} . We will describe how the M_{BH} and λ_{Edd} are related to M_{UV} for performing the integration with respect to M_{UV} (§ 2.2.2), and how the evolution of the UVLF Φ is modeled (§ 2.2.1).

The optical depth for a photon with an observed frequency ν traveling from z' to z , $\tau_X(z, z', \nu)$, is

$$\begin{aligned} \tau_X(z, z', \nu) &= \int_z^{z'} d\hat{z} \frac{c(1+\hat{z})^2}{H} \left(f_{\text{HI}} n_{\text{H}} \sigma_{\text{HI}}(\hat{\nu}) \right. \\ &\quad \left. + f_{\text{HeI}} n_{\text{He}} \sigma_{\text{HeI}}(\hat{\nu}) + f_{\text{HeII}} n_{\text{He}} \sigma_{\text{HeII}}(\hat{\nu}) \right) \end{aligned} \quad (14)$$

where $\hat{\nu} = \nu(1+\hat{z})/(1+z)$. We note that, to obtain Eq. (14) we assume that the HI distribution in the Universe is uniform. The inhomogeneity of the IGM grows during the EoR and might affect the process of the EoR (Khaire et al. 2016). However it is difficult to evaluate the effect of the inhomogeneity appropriately because the inhomogeneity during the EoR is highly uncertain. The distribution of Lyman limits

| z | α | β | M_* | $\log \Phi_*$ |
|------|----------------------|---------|-------|---------------|
| 2.00 | -1.5 | -3.76 | -25.4 | -5.86 |
| 4.25 | α_{hz} | -3.13 | -23.2 | -4.89 |
| 4.75 | α_{hz} | -3.14 | -23.6 | -5.36 |
| 5.75 | α_{hz} | -3.35 | -23.4 | -5.38 |
| 8.00 | α_{hz} | -3.73 | -23.0 | -5.43 |
| 10.0 | α_{hz} | -3.99 | -22.8 | -5.47 |

Table 1. Parameters of our AGN UVLF model at $z = 2.0, 4.25, 4.75, 5.75, 8.00,$ and 10.0 . The faint-end slope α_{hz} at $z > 4.25$ is a parameter. The $\log \Phi_*$ is for $z_{\text{AGN}} = 6.0$.

system at the EoR, which are one of main absorber of the IGM, is still unknown, although those at $z < 6$ are well studied (Inoue et al. 2014). Cosmological simulations usually show that the IGM tends to be uniform with increasing redshift (e.g. Iliev et al. 2006). We will discuss the impact of the IGM inhomogeneity on our results in § 4.

2.2.1 AGN luminosity function

UVLFs of AGNs have been actively studied by using large sample data from various surveys. However the UVLFs of high- z faint AGNs still has large uncertainties. In this paper, we construct an AGN UVLF model consistent with recent observations. According to Croom et al. (2009), we express the UVLF in the shape of double power-law as

$$\Phi(z, M_{\text{UV}}) = \frac{\Phi_* \exp(-z/z_{\text{AGN}})}{10^{0.4(\alpha+1)(M_{\text{UV}}-M_*)} + 10^{0.4(\beta+1)(M_{\text{UV}}-M_*)}}. \quad (15)$$

Here the parameters Φ_* , M_* , α and β respectively control the amplitude, characteristic M_{UV} where the slope switches, faint-end slope, and bright-end slope of the UVLF. These parameters are set to reproduce observed UVLFs at $z < 4$ (Croom et al. 2009; Giallongo et al. 2015). In Eq. (15), z_{AGN} controls the decrease of AGNs at high- z and which is set as $z_{\text{AGN}} = 6$.

The details of UVLFs at higher redshifts are still under debate, especially in their faint-end parts. Our aim of this paper is to evaluate these contributions to the EoR process. Therefore, we introduce a parameter α_{hz} as the faint-end slope parameter at $z > 4.25$. Then we interpolate α between $z = 2$ and $z = 4.25$. For other UVLF parameters, i.e. Φ_* , M_* , and β in high redshifts $z > 4.25$, we take the $\log(1+z)$ interpolation using the values at redshifts $z = 4.25, z = 4.75$ and $z = 5.75$ represented in Giallongo et al. (2015). We further extrapolate these parameters for $z > 5.75$. The UVLF parameters used in this paper are listed in Table 1. We show our AGN UVLF models for different redshifts at Fig. 1. Our UVLF models are well consistent with observations at each redshift. As shown by the right panel of the figure, the contribution of faint AGNs to reionization increases with decreasing α_{hz} and increasing $M_{\text{UV}}^{\text{min}}$.

2.2.2 AGNs spectral energy distribution

In this section, we derive an SED model depending on M_{BH} and λ_{Edd} based on results by Kawaguchi et al. (2001) who have numerically computed the SED of a system composed of the standard accretion disk and coronal gas. Hereafter we

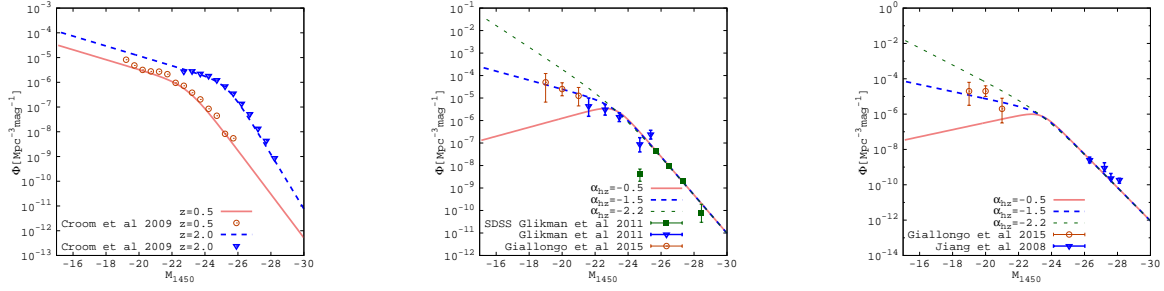


Figure 1. AGN UVLFs at $z < 2$ (left), $z = 4.25$ (center), and $z = 5.75$ (right). Observational data are taken from Jiang et al. (2008); Croom et al. (2009); Glikman et al. (2011); Giallongo et al. (2015). In the central and right panels, modeled LFs with $\alpha_{\text{hz}} = 0.0, -1.3,$ and -2.2 are respectively shown by the red thick solid, blue thick dashed, and green thin dashed lines.

call this model as the AC model (accretion disk + corona). We firstly introduce a shape function $\phi(E)$ as

$$\nu L_\nu = L_{\text{UV}} \phi(E), \quad (16)$$

$$\phi(E) = \left\{ \left(\frac{E}{E_1} \right)^{\gamma_a} + \left(\frac{E}{E_1} \right)^{\gamma_b} \right\}^{-1} + A_c \left\{ \left(\frac{E}{E_2} \right)^{\gamma_c} + \left(\frac{E}{E_2} \right)^{\gamma_d} \right\}^{-1} \quad (17)$$

where L_{UV} , A_c , γ_a , γ_b , γ_c , γ_d , E_1 , and E_2 are the model parameters that are selected for reproducing the SED with $M_{\text{BH}} = 3 \times 10^9 M_\odot$ and $\lambda_{\text{Edd}} = 0.05$ obtained in Kawaguchi et al. (2001)¹. Carrying out the χ^2 fitting, the parameters are found to be $A_c = 0.397$, $\gamma_a = -0.0191$, $\gamma_b = 0.685$, $\gamma_c = -0.255$, $\gamma_d = 0.211$, $E_1 = 9.44 \times 10^3$ keV, $E_2 = 1.22 \times 10^{-3}$ keV, and $L_{\text{UV}} = 3.4 \times 10^{45}$ erg/s.

We employ the scaling relations theoretically motivated in Kawaguchi et al. (2001) to take the dependence of the SED on M_{BH} and λ_{Edd} into account. According to the standard accretion disk model, the peak frequency of the big blue bump (the bump of the left-hand side in the SED) follows the scaling relation,

$$\nu_p \propto M_{\text{BH}}^{-1/4} \lambda_{\text{Edd}}^{1/4}. \quad (18)$$

In addition, the scaling of the total luminosity is simply given by

$$L = \lambda_{\text{Edd}} L_{\text{Edd}} \propto \lambda_{\text{Edd}} M_{\text{BH}}. \quad (19)$$

Kawaguchi et al. (2001) have indeed shown that these simple relations approximately explain the behavior of their computed SEDs.

Owing to the scaling relations, we can uniquely convert $L_\nu(M_{\text{BH}}, \lambda_{\text{Edd}})$ into $L_\nu(M_{\text{UV}})$ appearing in Eq. (13) with taking λ_{Edd} . As the redshift evolution of λ_{Edd} We adopt $\lambda_{\text{Edd}}(z) = \min[0.0091 \times (1+z)^{1.9}, 1.0]$ based on observations by Shen & Kelly (2012).

In order to discuss the impact of the shape of the SED on the reionization history, we also perform calculations with a simple power-law SED (hereafter the PL model) proposed by Lusso et al. (2015),

$$L_\nu \propto \begin{cases} \nu^{-0.61}, & h_p \nu < 13.6 \text{ eV}, \\ \nu^{-1.70}, & h_p \nu \geq 13.6 \text{ eV}, \end{cases} \quad (20)$$

which is employed in Madau & Haardt (2015). Also

¹ To be exact, there is a degeneracy between λ_{Edd} and the radiation efficiency η . We implicitly assume $\eta = 0.1$ for the fiducial model.

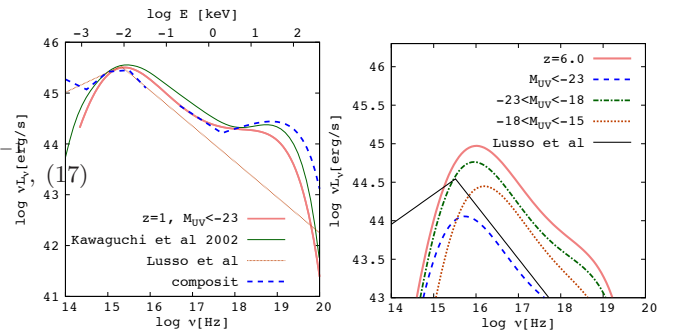


Figure 2. Left: Weighted average SED for AGNs at $z = 1$. The red thick solid curve represents AC model. The SED with $M_{\text{BH}} = 3 \times 10^9 M_\odot$ and $\lambda_{\text{Edd}} = 0.05$ computed by Kawaguchi et al. (2001) (green thin solid curve) and the observed composite SED (Zheng et al. (1997); Laor et al. (1997)) (blue thick dashed curve) are also plotted for reference. The PL model is shown by the thin dotted curve Lusso et al. 2015. Right: Weighted average SED for AGNs at $z = 6$ with $\alpha_{\text{hz}} = -1.5$. The AC model and the PL model are shown by the red thick and black thin solid curves, respectively. The blue dashed, green dot-dashed, and red dotted curves respectively represents the contribution from AGNs with $M_{\text{UV}} < -23$, with $-23 \leq M_{\text{UV}} < -18$, and with $-18 \leq M_{\text{UV}} < -15$. We note that the contribution from faint AGNs depends on α_{hz} .

Khaire et al. (2016) assumed a power-law SED which has different power. The amplitude of the PL model is determined to match its luminosity at the wavelength of 1450 to that of AC model. For comparison, we calculate the weighted average SED as

$$\overline{L_\nu}(\nu, z) = \frac{\int \Phi(M_{\text{UV}}, z) L_\nu(M_{\text{UV}}) dM_{\text{UV}}}{\int \Phi(M_{\text{UV}}, z) dM_{\text{UV}}}. \quad (21)$$

for each model and show the results in Fig. 2. We find that AC model has higher ionizing photon emissivity at $z = 6$ due to the dependence of the peak frequency on M_{BH} and λ_{Edd} shown in Eq. (18).

2.2.3 AGNs emissivity at 13.6eV

The AGN hydrogen ionizing emissivity ε_{912} , namely the emissivity of AGNs at $E = 13.6$ eV, is a good indicator to represent how much photons emitted from AGNs contribute to the cosmic reionization process. By using Eq. (13) with

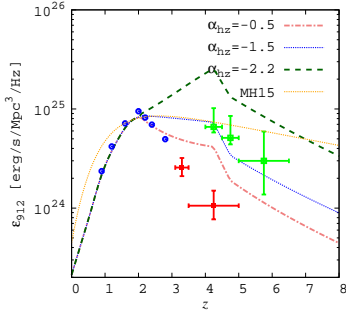


Figure 3. Parameter dependence of AGN emissivity. We show AGN ionizing emissivity inferred from Masters et al. (2012) in red, Giallongo et al. (2015) in green and Palanque-DeLabrouille et al. (2013) in blue.

our LF and SED models, we calculate ε_{912} and plot the redshift evolution for different α_{Hz} in Fig. 3.

The luminosity of AGNs over the wide redshift range are obtained through many independent observations. Following Eq. (3) in Giallongo et al. (2015), we calculate ε_{912} for different observations. Palanque-DeLabrouille et al. (2013) have provide the g-band luminosity function in the redshift range, $0.68 < z < 4$, from SDSS-III and Multiple Mirror Telescope data. We plot ε_{912} obtained from Palanque-DeLabrouille et al. (2013) as blue circles in Fig. 3. Masters et al. (2012) have also yielded the high- z quasar luminosity function from the Cosmic Evolution Survey (COSMOS). Their result suggests a characteristic decrease of quasar number density from $z=3$ to 4 and we show their ε_{912} in red points of Fig. 3. Green squares in Fig. 3 are obtained from the UV luminosity function of faint AGNs at $4 < z < 6.5$ found by Giallongo et al. (2015). Although they used only 22 AGN candidates in the CANDLES GOODS-South field as samples, their result is obviously different from that by Masters et al. (2012),

As shown in Fig. 3 the AGN emissivity in $z \approx 4$ has a large uncertainty. This is because the sample sets of AGNs in each observation are not consistent with each other. Furthermore, the uncertainty of the AGN emissivity increases in $z > 6$ since there are few samples of high- z AGNs. Due to large uncertainty, the measurement of the AGN ionizing emissivity cannot put a strong constraint on the evolution factor α_{Hz} .

Before the comparison with the EoR observation data in next section, we show the AGN emissivity at $z < 15$ for different α_{Hz} with AC and PL model. Fig. 4 shows that thick lines corresponding to the emissivity for our AC model is larger than thin lines corresponding to the emissivity for the PL model. For the reference, we also plot the AGN dominant model in MH15 as the dot-dashed line.

3 RESULTS

Hereafter, we treat α_{Hz} is a free parameter since the AGN abundance has a large uncertainty at $z > 4$. The escape fraction f_{esc} is also highly uncertain because direct measurement of f_{esc} is difficult. Thus, we compare our results with the ob-

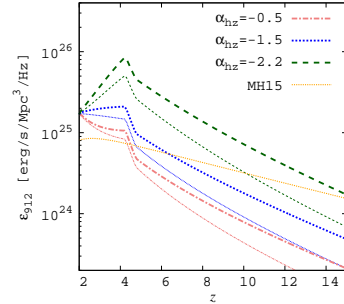


Figure 4. AGN emissivity for AC model (thick lines) and PL model (thin lines) for $\alpha_{\text{Hz}} = -0.5, -1.5$ and -2.2 . The dot-dashed line shows the model in MH15.

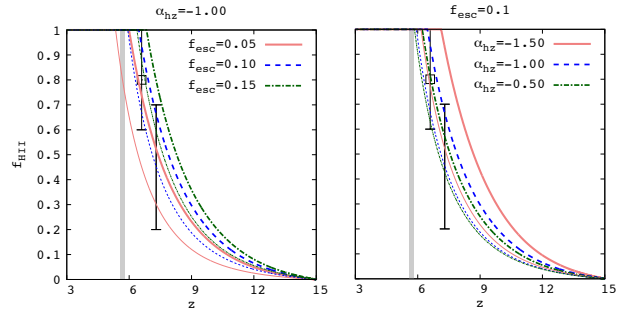


Figure 5. HI ionizing history with various sets of f_{esc} and α_{Hz} . The completion of the HI reionization at $z = 5.7$ is indicated by the gray vertical line. Two data points with error bars represent the constraints from the LAE observations (Ouchi et al. 2010; Konno et al. 2014). Thin lines represent HI ionizing history with same parameter sets and PL model.

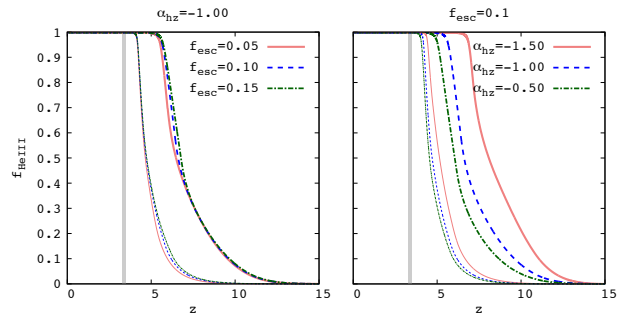


Figure 6. HeII ionizing history with various sets of f_{esc} and α_{Hz} . The completion of the HeII reionization at $z = 3.4$ is indicated by the gray vertical line (Worseck et al. 2014). Thin lines represent HeII ionizing history with same parameter sets and PL model.

servational data of HI and HeII ionizing history, Thomson optical depth of the CMB in order to obtain constraints on these parameters.

3.1 the reionization evolution with f_{esc} and α_{Hz}

Before the comparison with the EoR observations, we first show the dependence of the reionization evolution on the parameters f_{esc} and α_{Hz} . Fig. 5 represents the HI ionizing

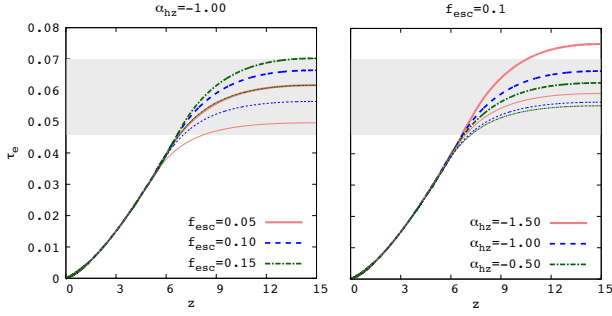


Figure 7. CMB Thomson optical depth with various sets of f_{esc} and α_{hz} . A constraint from the CMB observation, $\tau_e = 0.058 \pm 0.012$ is shown as a gray region (Planck Collaboration et al. 2016). Thin lines represent CMB Thomson optical depth with same parameter sets and PL model.

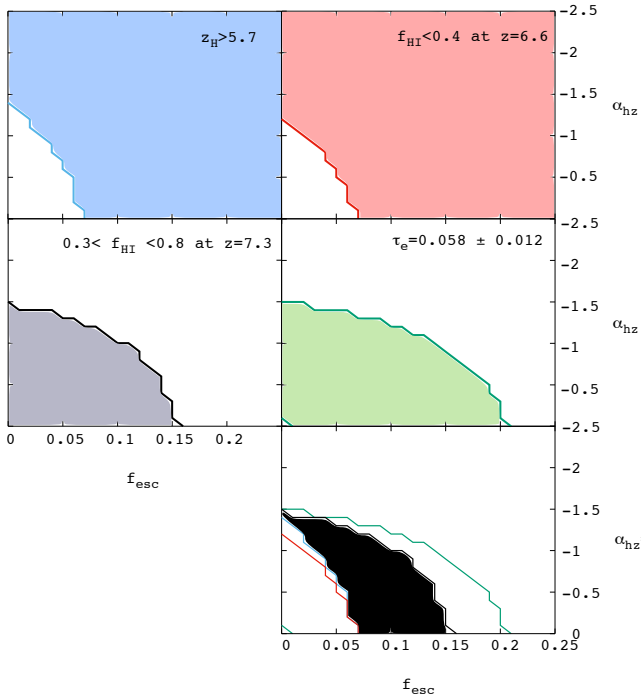


Figure 8. Constraints on the parameters, f_{esc} and α_{hz} , from the observations: the redshift of the completion of the hydrogen reionization $z_{\text{H}} > 5.7$ (top left), the neutral fraction $f_{\text{HI}} < 0.2 \pm 0.2$ at $z = 6.6$ (top right), $0.3 < f_{\text{HI}} < 0.8$ at $z = 7.3$ (middle left) the Thomson optical depth of the CMB $\tau = 0.058 \pm 0.012$ (middle right). The black region in the bottom panel is the combined allowed region.

history for different sets of f_{esc} and α_{hz} . As we can see, higher values of f_{esc} and α_{hz} increase the number of ionizing photons and result in the earlier completion of the HI reionization.

Fig. 6 represents the HeII reionization for different sets of f_{esc} and α_{hz} . Because of the existence of X-ray photons, AGNs can ionize HeII more effectively than galaxies. Therefore, HeII ionizing history has a stronger dependence on α_{hz} than on f_{esc} as shown in Fig. 6.

The CMB optical depth to Thomson scattering is a good probe for the evolution of the EoR. The optical depth is

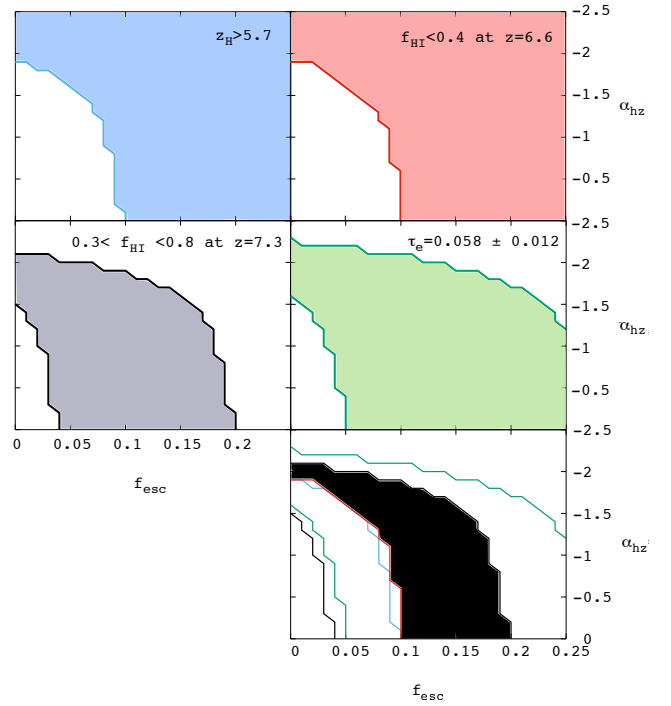


Figure 9. Constraints on the parameters, f_{esc} and α_{hz} , same as Fig. 8 but for PL model.

obtained as

$$\tau_e(z) = \int_0^z c\sigma_{\text{T}}n_e(1+z)^3 \frac{dt}{dz} dz, \quad (22)$$

where σ_{T} is Thomson cross section. Fig. 7 shows the dependence of τ_e on the parameter set of f_{esc} and α_{hz} . The optical depth τ_e does not change after the HI reionization was completed. This is because almost all of photon-scattering electrons are produced by hydrogen ionization. Therefore, τ_e is sensitive to the hydrogen reionization process.

3.2 constraints on the model parameters

There are several observations which provide constraints on the evolution of cosmological reionization process. From the comparison with our results, we can obtain constraints on the parameter set of f_{esc} and α_{hz} . The observations of the spectra of high- z quasars suggest that the cosmic reionization of HI is completed by $z = 5.7$ (Fan et al. 2006). Therefore, we set the criterion for the completion of HI reionization as $f_{\text{HI}} = 0.9999$ at $z_{\text{H}} = 5.7$. Ouchi et al. (2010) provided the constraint on the neutral fraction of $f_{\text{HI}} < 0.2 \pm 0.2$ at $z = 6.6$ from the observation of LAEs. Further, Konno et al. (2014) indicated $0.3 < f_{\text{HI}} < 0.8$ at $z = 7.3$ from a drastic decrease in the number of LAEs. Thus, the observations of LAEs and QSOs give the upper limit on the HI fraction and set minimum amounts of ionizing sources. As we can see in top panels of Fig. 8, they provide lower bounds on f_{esc} and α_{hz} . On the other hand, the lower bound on the HI fraction at $z = 7.3$ constrains the models with large values of f_{esc} and α_{hz} as shown in the middle left panel of Fig. 8. In addition, the boundary curves become vertical for large values of α_{hz} . This is because galaxies are dominant sources of ion-

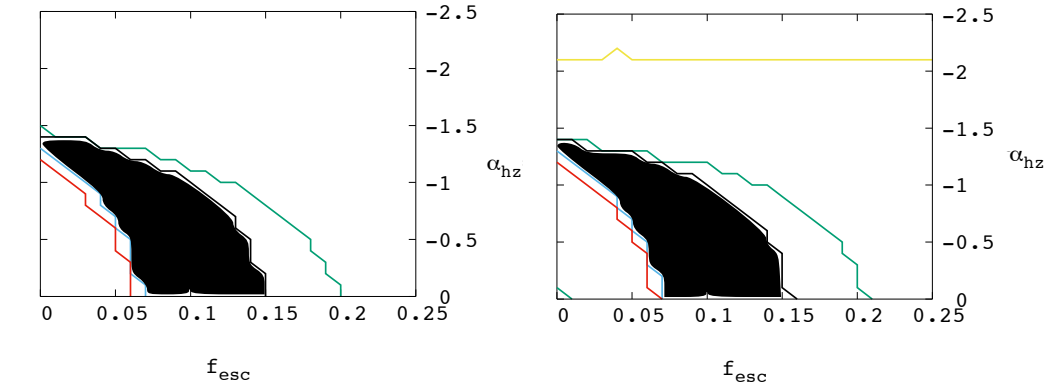


Figure 10. Constraints on the parameters, f_{esc} and α_{hz} for two kind of models with $z_{\text{AGN}} = 10$ (left) and $M_{\text{min}} = -15$ (right). The black regions are combined allowed regions.

izing photons and the ionization history is not affected by α_{hz} .

Next we focus on the HeII reionization. The effective optical depth for HeII Lyman- α absorption suggests that almost all of helium in IGM are fully ionized at $z > 3.4$ and $f_{\text{HeII}} = 0.003$ was obtained at $z=3.4$ (Worseck et al. 2014). Therefore, we can assume that the HeII reionization is completed when the HeIII fraction exceeds $f_{\text{HeIII}} = 0.997$ and this redshift is written as z_{He} . The measurement of the effective optical depth for HeII Lyman- α provides the upper limit on HeII fraction which provides the lower limit of the parameters f_{esc} and $a_{z=4}$. However, we adopt the LF model which has relatively abundant AGNs at $z = 4$. The AGN emissivity is sufficiently large to ionize HeII by $z = 3.4$ even if $\alpha_{\text{hz}} = 0.0$. Therefore, HeII reionization does not put useful constraints on our parameters.

The Planck observation (Planck Collaboration et al. 2016) measured the CMB optical depth for Thomson scattering and provided $\tau_e = 0.058 \pm 0.012$. In Fig. 7 we plot lower and upper bounds on τ_e . Since the optical depth depends on f_{esc} and α_{hz} , we obtain the constraint on these parameters. We plot the upper and lower bounds on f_{esc} and α_{hz} as shown in the bottom left panel of Fig. 8.

Combining the above constraints, we obtain the bottom right panel of Fig. 8 which shows the parameter sets satisfying all constraints. As we can see, the evolution factor of the faint end slope of the AGN LF should be $\alpha_{\text{hz}} < -1.5$ and the escape fraction must satisfy $f_{\text{esc}} < 0.13$. Here, the total constraint is mostly contributed from the observations of the HI fraction at $z = 6.6$ and 7.3 . This result implies that high AGN abundance at high redshifts reported in Giallongo et al. (2015) is not allowed unless the contribution of galaxies is very small ($f_{\text{esc}} < 0.05$, see Fig. 3). Nevertheless, an ‘‘AGN-dominant scenario’’ is still viable for $\alpha_{\text{hz}} \approx -1.5$ which implies that faint AGNs are less abundant than the model adopted in MH15. The allowed values of f_{esc} is relatively smaller than it was predicted in the previous works. This is because the AGNs with AC model has non-negligible contribution to ionization.

Besides, in order to see the effect of the SED shape on the results, we compare them with those with the PL model. Thin lines in Figs. 5 to 7 represent the evolution of HII/HeIII fraction and τ_e for models with the PL SED and same parameter sets as used for the fiducial model. First, in Fig. 5,

the whole HI ionizing history is delayed. This indicates that, for the PL model, AGNs can not ionize the HI as effectively as the AC model. Then, the constraints from HI reionization and HI fraction shift in the upper direction in the panels of Fig. 9.

Second, similarly, the whole HeII ionizing history is delayed. AGNs in the PL model emit less HeII ionizing photons than the fiducial model. However, as in the case of AC model, the HeII reionization does not lead to a useful constraint on the model parameters.

Third, the difference of τ_e from the fiducial model reflects the delay in the ionizing history. Thus, the τ_e of the PL model is less than the τ_e of the fiducial model. Consequently, τ_e provides not only upper bounds but lower bounds on the model parameters in the top middle panel of Fig. 9.

As a result, as we can see in the bottom right panel of Fig. 9, the combination constrains the parameters as $f_{\text{esc}} < 0.21$ and $\alpha_{\text{hz}} > -2.0$. This result allows the existence of more faint AGNs ($-1.5 > \alpha_{\text{hz}} > -2.0$) at high redshifts as suggested in Giallongo et al. (2015) when the value of f_{esc} is less than 0.07. Besides, for a model with $\alpha_{\text{hz}} > -1.0$ has $0.1 < f_{\text{esc}} < 0.2$ which is larger than the case of the AC model and is consistent with the previous works (e.g. Wise et al. (2014); Kimm & Cen (2014); Khaire et al. (2016)). This indicates the AGNs for the PL model ionize HI less effectively and therefore, a larger contribution from galaxies is required.

As stated above, the AGN contribution is much sensitive to SED model. Thus, the construction of realistic SED model is crucial for proper estimation of the ionization history and parameters.

4 DISCUSSION

4.1 Model uncertainty

In this subsection, we discuss the uncertainties in our model. First, let us consider the SED and LF of AGNs. We assumed that the SED depends on the Eddington ratio λ_{Edd} and all AGNs have the same value for a fixed redshift. However, dependence of λ_{Edd} on AGN luminosity is reported (e.g. Collin & Kawaguchi (2004); Nobuta et al. (2012)). However, we ignored the dependence since it has large variance. For example, when faint (bright) AGNs have relatively small

(large) value of λ_{Edd} , their ionization efficiency would become smaller (larger). Then, the constraint on α_{hz} will become weaker if we take this effect into account because the contribution of faint AGNs reduces.

Next, concerning star forming galaxies, we used a fixed SFRD model. However, the SFRD depends on the faint-end shape and dust correction of UV luminosity functions. Although some recent observation indicated the observational faint-end limit of UV magnitude $M_{\text{UV}} = -17$ and the faint-end slope $\alpha = -2$ at $z > 6$ (Ishigaki et al. 2015; Bouwens et al. 2015), UV luminosity functions during the EoR are still less well-known. For instance, Ishigaki et al. (2015) showed that the SFRD integrated down to $M_{\text{UV}} = -10$ is larger than one down to $M_{\text{UV}} = -17$ by a factor of 3, assuming $\alpha = -2$. Our SFRD model (Madau & Dickinson 2014) was obtained by integration of luminosity function down to $0.03L^*$, where L^* is the characteristic luminosity of the Schechter function. Further, the dust correction causes a variation by a factor of 2 to the SFRD (Hopkins & Beacom 2006). Additionally, a rapid decrease in the SFRD at $z > 8$ is indicated from a recent observation (Bouwens et al. 2015). Thus, the contribution of galaxies to the HI reionization at $z > 8$ may be overestimated in our calculations. For these reasons, the SFRD has an uncertainty of a factor of $2 \sim 6$. In our calculation, we can consider this uncertainty was incorporated in f_{esc} .

Finally, let us see the effect of the inhomogeneity of the IGM. We treated the IGM as being uniform in our calculations, however the observed Universe is obviously inhomogeneous. The effective optical depth τ_{eff} through the inhomogeneous medium is estimated as an integration of the HI distribution function and the continuum optical depth with respect to HI column density (Haardt & Madau 2012). In Inoue et al. (2014), they reported the distribution function of intergalactic absorbers (IGA) $F_{\text{IGA}}(z) = \partial^2 n / \partial z \partial N_{\text{HI}}$ at $z < 6$ and gave an analytic model. Khaire et al. (2016) have shown that an HI distribution function derived from a cosmological hydrodynamic simulation well corresponds to the analytic model by Inoue et al. (2014) at $z = 5 - 6$, and used it for computing the reionization history. Despite the efforts by these studies, there is still large uncertainty in the HI distribution function during the EoR; we should estimate it to be consistent with the reionization process that affects the HI distribution function. Since constructing the complete model is very tough work, we evaluate the impact of the inhomogeneity with a simple model. We adopt the analytic model by Inoue et al. (2014) in post-reionization epoch and extrapolate to higher redshifts as $F_{\text{IGA}}(z) = F_{\text{IGA}}(z = 5.7) (f_{\text{HI}}(1 + f_{\text{HII}}^{\text{ion}}) / f_{\text{HII}}^{\text{ion}}(1 - f_{\text{HII}}^{\text{ion}})) ((1 + z) / (1 + 5.7))^2$. Here, $f_{\text{HII}}^{\text{ion}} = 3 \times 10^{-3}$ corresponds to the mass weighted ionized fraction at $z = 5.7$ (Fan et al. 2006). For simplicity, we assume that the distribution of HeI and HeII follows the HI distribution. Therefore, we estimate the column density of HeI and HeII as $N_{\text{HeI}} = (f_{\text{HeI}} / (f_{\text{HI}} + f_{\text{HII}}^{\text{ion}})) (n_{\text{He}} / n_{\text{H}}) N_{\text{HI}}$ and $N_{\text{HeII}} = (f_{\text{HeII}} / (f_{\text{HI}} + f_{\text{HII}}^{\text{ion}})) (n_{\text{He}} / n_{\text{H}}) N_{\text{HI}}$. As a result, as we can see in Fig. 11, a model with $f_{\text{esc}} = 0.05$ and $\alpha_{\text{hz}} = -1.00$ completes HI reionization at $z_{\text{H}} = 5.58$ in clumpy universe, while the completion is at $z_{\text{H}} = 6.02$ for uniform IGM. Therefore, the appropriate value of f_{esc} (α_{hz}) may become larger (smaller) than our results if we incorporate the inhomogeneity of the IGM.

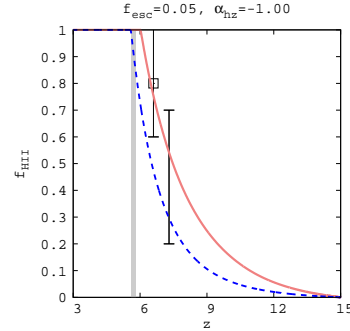


Figure 11. HI ionization history homogeneous (solid line) and inhomogeneous (dashed line) IGM.

4.2 Remaining parameters

In this work, we mainly focused on f_{esc} and α_{hz} . However, our model has two other parameters, z_{AGN} and the faint end of UV luminosity $M_{\text{UV}}^{\text{min}}$.

Firstly, we discuss the z_{AGN} which determines the critical redshift of AGN abundance decrease at higher redshifts. This parameter relates to many interesting questions on the origin of the first AGNs. The value of z_{AGN} would be larger than 6 where AGNs have been observed, but it is highly uncertain. When we set $z_{\text{AGN}} = 10$ rather than our fiducial value $z_{\text{AGN}} = 6$, AGNs ionize HI strongly at higher redshifts. In the left panel of Fig. 10, we show the allowed parameter region for a model with $z_{\text{AGN}} = 10$. Consequently, the result is not different significantly with the fiducial one.

Secondly, we discuss the faint end of the AGN UV luminosity function. Although a faint AGN with $M_{\text{UV}} = -19$ has been found at $z = 5.75$ in Giallongo et al. (2015), the faint end has not been well determined observationally even at lower redshifts. However, we did not treat $M_{\text{UV}}^{\text{min}}$ as a main parameter in this work. This is because for a value of the faint-end slope of interest ($\alpha_{\text{hz}} > -2.0$), faintest AGNs ($-18 < M_{\text{UV}} < -15$) do not significantly contribute to the total AGN luminosity as can be seen in the right panel of Fig. 2. Therefore, the results are expected to be rather insensitive to the value of the faint end. This can be confirmed in the right panel of Fig. 10 where the faint end is set to $M_{\text{UV}}^{\text{min}} = -15$ rather than the fiducial value of -18.

4.3 Cosmic X-ray background

As we saw, high-redshift AGNs can significantly contribute to the reionization of intergalactic hydrogen and helium. Then there is a possibility that they contribute to X-ray background (XRB) as well. In this subsection, we estimate the XRB originated from AGNs and discuss whether the observed XRB (Choudhury & Ferrara 2005; Frontera et al. 2007; Gruber et al. 1999; Ajello et al. 2008) can place an additional constraint on the parameter of AGN abundance. Particularly, the AC model leads to strong X-ray emission and easy to exceed the observed upper limit. In Fig. 12, we show the spectrum of the XRB, $I(E)$ [$\text{keV}^2 \text{cm}^{-2} \text{s}^{-1} \text{keV}^{-1} \text{Str}^{-1}$], estimated from the AGN flux,

$$I[E] = E \frac{F(z, \nu_0)}{4\pi h}. \quad (23)$$

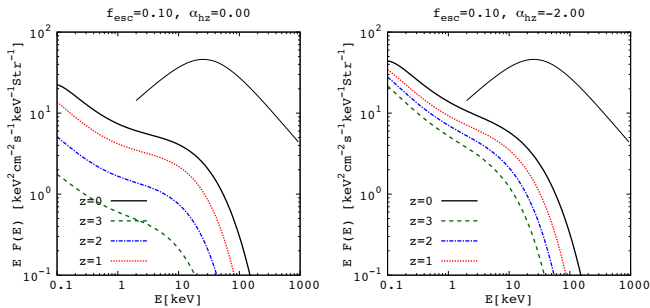


Figure 12. Cosmic X-ray background spectrum for our constrained model. The solid line corresponds to the XRB at $z = 0$ which is based on parameters showed above this figure. The best fit XRB spectrum (thin solid line) obtained in Ajello et al. (2008) is plotted for reference. The XRB of our result does not exceed the upper limit calculated by using equation 5 in Ajello et al. (2008). Other lines are the XRB calculated at several redshifts.

Simultaneously, we plot the XRB calculated at several redshifts and an upper limit from Ajello et al. (2008). As we can see, even if we vary α_{hz} significantly ($\alpha_{\text{hz}} = 0.0$ and -2.0), the amount of the XRB at $z = 0$ does not exceed the upper limit. This is because the photons emitted from low redshifts AGNs ($z < 3$) are dominant in the XRB and those from the high- z AGNs can contribute to the XRB by only 1% at most. Therefore, XRB is not able to constrain AGN abundance at $z > 3$.

4.4 Radio loud quasars

If AGNs were too abundant and bright in radio frequency range in high redshift, their emission would serve as a background of the 21cm line of neutral hydrogens. In this subsection we estimate, using our constrained AGN model, the number of photons that radio loud QSOs would emit at radio frequency range and compare it to that of the CMB. We base our estimation on the result of Elvis et al. (1994); Prieto et al. (2010), in which the authors found SED of radio loud QSOs at radio frequency range to be 2-3 orders of magnitude smaller than the SED at UV frequency range ($1.25\mu\text{m}$). Remembering that the intensity ratio between at $1.25\mu\text{m}$ and 1keV is approximately $10^{-0.4}$, it is expected that the intensity ratio between at 21 cm and 1 keV is about $\sim 10^{-2}$. Setting the ratio as $10^{-\alpha}$ ($\alpha = 2$ is the fiducial value), we write the SED at 21 cm line frequency as

$$\frac{F_{\nu_{21}}}{4\pi} = \frac{10^\alpha}{4\pi} \left(\frac{\nu_{21\text{cm}}}{\nu_{1\text{keV}}} \right) F_{1\text{keV}} \quad (24)$$

$$= \frac{10^\alpha}{\nu_{21\text{cm}}} I_{\nu_{1\text{keV}}} [\text{keV s}^{-1} \text{ Hz}^{-1} \text{ cm}^{-2} \text{ str}^{-1}] \quad (25)$$

$$= 1.14 \times 10^{5-\alpha} I_{\nu_{1\text{keV}}} [\text{Jystr}^{-1}]. \quad (26)$$

The conversion formula from intensity to brightness temperature is given by

$$\left(\frac{T_b}{\text{K}} \right) = 3.255 \times 10^{-5} \left(\frac{\nu}{\text{GHz}} \right)^2 \left(\frac{F_\nu/4\pi}{\text{Jy str}^{-1}} \right). \quad (27)$$

From the above equations and Fig. 12, we can estimate that $I_{\nu_{1\text{keV}}} < 100$ at $z = 0$, and $T_b < 370 \times 10^{-\alpha} [\text{K}]$ in terms of brightness temperature. If we assume that the AGNs are all radio loud QSOs ($\alpha = 2$), this estimate gives $T_b < 3.7 \text{ K}$.

At higher redshifts of interest ($z > 6$) the intensity should be a few orders of magnitude smaller, and therefore, the contribution of radio loud AGNs to the background of 21cm line should be negligible compared to the CMB ($T_\gamma = 2.7(1+z)$).

4.5 Thermal history

We can calculate not only the ionization history but also the thermal history of the IGM with our model. The ionizing history is affected by the thermal state of the ionized gas through the recombination coefficient. If we assume the fixed IGM temperature of 20,000 [K] as is in HM15 for a model with $f_{\text{esc}} = 0.10$ and $\alpha_{\text{hz}} = -0.50$, z_{H} and τ_e increase by 0.12 and 1.0×10^{-3} respectively.

Besides, in Fig. 13, we show the HI ionizing history and the thermal history for two representative sets of parameters in the allowed region. Although the f_{HII} history for a model with $f_{\text{esc}} = 0.05$ and $\alpha_{\text{hz}} = -1.00$ is almost the same for a model with $f_{\text{esc}} = 0.10$ and $\alpha_{\text{hz}} = 0.00$, the IGM temperature of the former is higher than that of the latter. This is because the heating efficiency of AGNs is much higher than galaxies and a model with more AGNs results in higher IGM temperature. Thus, the thermal history could be another probe of ionization sources.

Furthermore, we show the ionization and thermal history of a model with $z_{\text{AGN}} = 10.0$ and the PL model. The parameters f_{esc} and α_{hz} are chosen so that similar evolution of f_{HII} is realized. The IGM temperature of the model with $z_{\text{AGN}} = 10$ at $z > 10$ is higher than that of the fiducial model with the same values of f_{esc} and α_{hz} because the larger value of z_{AGN} leads to high AGN emissivity at high redshifts. On the other hand, the models with the PL model show different thermal histories. This is because, for these models, AGNs radiate relatively smaller amount of high-energy photons compared to the AC models, fixing the amount of ionizing photons. These differences in the IGM temperature can be an indicator of the existence of AGNs at high redshifts and a probe of the SED.

The thermal history is imprinted on 21cm-line signals from neutral hydrogen through the spin temperature. The 21cm-line signals are a major target of the SKA and its pathfinders such as the MWA and LOFAR. Especially, statistical quantities such as the power spectrum, bispectrum, variance and skewness are expected to be able to probe the fluctuation in the 21cm brightness temperature (Madau et al. 1997; Tozzi et al. 2000; Furlanetto et al. 2006; Pritchard & Furlanetto 2007; Pober et al. 2014; Baek et al. 2010; Shimabukuro et al. 2015; Yoshiura et al. 2015).

5 CONCLUSION

In this work, we studied the HI and HeII reionization with a simple model of star forming galaxies and AGNs. We compared the observational data on the HI and HeII fraction and CMB optical depth with our model and obtained constraints on the escape fraction of ionizing photons, f_{esc} , and the faint-end slope of the AGN luminosity function at $z > 4.25$, α_{hz} . As a result, we have found that models with $\alpha_{\text{hz}} > -1.5$ and $f_{\text{esc}} < 0.15$ are consistent with the existing observations and the constraints come mostly from the HI fraction history

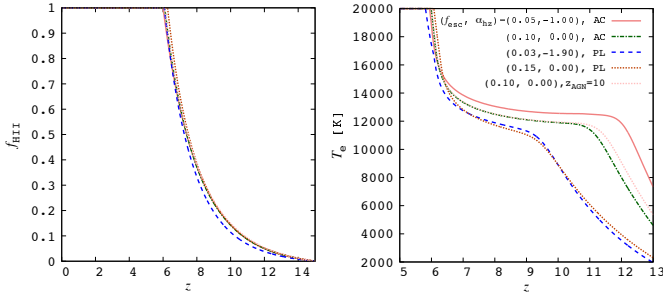


Figure 13. (Left) Evolution of the HII fraction for our constrained models with two typical sets of the parameters ($f_{\text{esc}}, \alpha_{\text{hz}}$)=(0.05, -1.00) and (0.10, 0.00). A model with the PL model and ($f_{\text{esc}}, \alpha_{\text{hz}}$)=(0.03, -1.90), and a model with ($f_{\text{esc}}, \alpha_{\text{hz}}$)=(0.15, 0.00) and $z_{\text{AGN}} = 10$ are also shown. (Right) Thermal history for the same models.

and the Thomson optical depth. Our result suggests that an AGN-dominated model with AGN abundance as large as the estimation in (Giallongo et al. 2015) is allowed, while a galaxy-dominated model is also allowed.

Besides, we have discussed that the XRB is not usable to constrain the parameters because the contribution of AGNs at $z > 3$ to the XRB is very small. Furthermore, even if we assume that the radio loud AGNs exist at high redshifts, the radiation is too small to serve as background emission of the 21cm-line signal of neutral hydrogen. Finally, we have calculated the thermal evolution of the IGM and found the α_{hz} changes the thermal history and the thermal evolution is sensitive to the abundance of AGNs and the shape of the SED. The 21cm-line observation will be useful to obtain more powerful constraints on the AGN abundance.

ACKNOWLEDGEMENT

We are grateful to A. K. Inoue for his suggestions regarding the model of AGNs, to T. Kawaguchi for kindly providing us with the theoretical and observational SED data, and to H. Shirakata for providing simulation results. We also thank the members of SKA-JP EoR science working group for fruitful discussion and comments. This work is supported by Grant-in-Aid from the Ministry of Education, Culture, Sports, Science and Technology (MEXT) of Japan, No. 26610048, No. 15H05896, No 16H05999 (K.T.), 24340048 (K.T., K.I.), No. 25-3015 (H.S.), 15K17646 (H.T.), 16J01585 (S.Y.). and a grant from NAOJ. H.T. also acknowledges the support by MEXT Program for Leading Graduate Schools PhD professional, ‘‘Gateway to Success in Frontier Asia’’.

REFERENCES

Ajello, M., Greiner, J., Sato, G., et al. 2008, *ApJ*, 689, 666
 Atek, H., et al. 2015, *ApJ*, 800, 81
 Baek, S., Semelin, B., Di Matteo, P., Revaz, Y., Combes, F. 2010, *A&A*, 523, A4
 Becker, G. D. and Bolton, J. S. and Haehnelt, M. G. Sargent, W. L. W. 2011, *MNRAS*, 410, 1096

Bouwens, R. J., Illingworth, G. D., Oesch, P. A., et al. 2015, *ApJ*, 803, 34
 Choudhury, T. R., Ferrara, A. 2005, *MNRAS*, 361, 577
 Collin, S., & Kawaguchi, T. 2004, *A&A*, 426, 797
 Croom, S. M., Richards, G. T., Shanks, T., et al. 2009, *MNRAS*, 399, 1755
 Dunlop, J. S., et al. 2013, *MNRAS*, 432, 3520
 Elvis, M., Wilkes, B. J., McDowell, J. C., et al. 1994, *ApJS*, 95, 1
 Fan, X., Strauss, M. A., Becker, R. H., et al. 2006, *AJ*, 132, 117
 Fukugita, M., Kawasaki, M. 1994, *MNRAS*, 269, 563
 Frontera, F., Orlandini, M., Landi, R., et al. 2007, *ApJ*, 666, 86
 Furlanetto, S. R., Oh, S. P., Briggs, F. H. 2006, *Phys. Rep.*, 433, 181
 Giallongo, E., Grazian, A., Fiore, F., et al. 2015, *A&A*, 578, A83
 Glikman, E., Djorgovski, S. G., Stern, D., et al. 2011, *ApJ*, 728, L26
 Gnedin, N. Y., Kravtsov, A. V., Chen, H.-W. 2008, *ApJ*, 672, 765
 Gruber, D. E., Matteson, J. L., Peterson, L. E., Jung, G. V. 1999, *ApJ*, 520, 124
 Hao, J.-M., Yuan, Y.-F., Wang, L. 2015, *MNRAS*, 451, 1875
 Haardt, F., & Madau, P. 2012, *ApJ*, 746, 125
 Hopkins, A. M., Beacom, J. F. 2006, *ApJ*, 651, 142
 Hu, E. M., Cowie, L. L., Barger, A. J., Capak, P., Kakazu, Y., Trouille, L. 2010, *ApJ*, 725, 394
 Iliev, I. T., Mellema, G., Pen, U.-L., Merz, H., Shapiro, P. R.; Alvarez, M. A. 2006, *MNRAS*, 369, 1625
 Inoue A. K., Shimizu I., Iwata I., Tanaka M., 2014, *MNRAS*, 442, 1805
 Ishigaki, M., Kawamata, R., Ouchi, M., Oguri, M., Shimasaku, K., Ono, Y., 2015, *ApJ*, 799, 12
 Iwata., et al. 2009, *ApJ*, 692, 1287
 Jiang, L., Fan, X., Annis, J., et al. 2008, *AJ*, 135, 1057
 Kashikawa, N., 2011, *ApJ*, 734, 119
 Kawaguchi, T., Shimura, T., Mineshige, S. 2001, *ApJ*, 546, 966
 Khaire, V., Srianand, R., Choudhury, T. R., & Gaikwad, P. 2016, *MNRAS*, 457, 4051
 Kimm, T., & Cen, R. 2014, *ApJ*, 788, 121
 Konno, A., Ouchi, M., Ono, Y., et al. 2014, *ApJ*, 797, 16
 Laor, A., Fiore, F., Elvis, M., Wilkes, B. J., McDowell, J. C. 1997, *ApJ*, 477, 93
 Lusso, E., Worseck, G., Hennawi, J. F., et al. 2015, *MNRAS*, 449, 4204
 Madau, P., & Dickinson, M. 2014, *ARA&A*, 52, 415
 Madau, P., & Haardt, F. 2015, *ApJ*, 813, L8
 Madau, P., Meiksin, A., & Rees, M. J. 1997, *ApJ*, 475, 429
 Masters, D., Capak, P., Salvato, M., et al. 2012, *ApJ*, 755, 169
 Mitra, S., Choudhury, T. R., & Ferrara, A. 2016, arXiv:1606.02719
 Nobuta, K., Akiyama, M., Ueda, Y., et al. 2012, *ApJ*, 761, 143
 Oesch, P. A. et al. 2014, *ApJ*, 786, 108
 Ota, K., et al. 2010, *ApJ*, 722, 803
 Ouchi, M., Mobasher, B., Shimasaku, K., et al. 2009, *ApJ*, 706, 1136
 Ouchi, M., Shimasaku, K., Furusawa, H., et al. 2010, *ApJ*, 723, 869
 Paardekooper, J.-P., Khochfar, S., Dalla Vecchia, C. 2009, *MNRAS*, 429, L94
 Palanque-Delabrouille, N., Magneville, C., Yèche, C., et al. 2013, *A&A*, 551, A29
 Pawlik, A. H., Schaye, J., van Scherpenzeel, E. 2009, *MNRAS*, 394, 1812
 Planck Collaboration, Ade, P. A. R., Aghanim, N., et al. 2015, arXiv:1502.01589
 Planck Collaboration, Adam, R., Aghanim, N., et al. 2016, arXiv:1605.03507
 Pober, J. C., Liu, A., Dillon, J. S., et al. 2014, *ApJ*, 782, 66
 Prieto, M. A., Reunanen, J., Tristram, K. R. W., Neumayer,

- N., Fernandez-Ontiveros, J. A., Orienti, M., Meisenheimer, K. 2010, MNRAS, 402, 724
- Pritchard, J. R., Furlanetto, S. R. 2007, MNRAS, 376, 1680
- Razoumov, A. O., Sommer-Larsen, J. 2010, ApJ, 710, 1239
- Raicević, M., Theuns, T. 2011, MNRAS, 412, L16
- Ricci, F., Marchesi, S., Shankar, F., La Franca, F., & Civano, F. 2016, arXiv:1610.01638
- Robertson, B. E., Ellis, R. S., Furlanetto, S. R., Dunlop, J. S. 2015, ApJ, 802, L19
- Shen, Y., & Kelly, B. C. 2012, ApJ, 746, 169
- Shimabukuro, H., Yoshiura, S., Takahashi, K., Yokoyama, S., Ichiki, K. 2015, MNRAS, 451, 467
- Steidel, C. C., Pettini, M., Adelberger, K. L. 2001, ApJ, 546, 665
- Siana, B., Shapley, A. E., Kulas, K. R., et al. 2015, ApJ, 804, 17
- Susa, H. 2006, PASJ, 58, 445
- Syphers, D., & Shull, J. M. 2014, ApJ, 784, 42
- Tozzi, P., Madau, P., Meiksin, A., & Rees, M. J. 2000, ApJ, 528, 597
- Ueda, Y., Akiyama, M., Hasinger, G., Miyaji, T., Watson, M. G. 2014, ApJ, 786, 104
- Wise, J. H., Demchenko, V. G., Halicek, M. T., Norman, M. L., Turk, M. J., Abel, T., Smith, B. D. 2014, MNRAS, 442, 2560
- Worseck, G., Prochaska, J. X., Hennawi, J. F., McQuinn, M. 2014, arXiv:1405.7405
- Yajima, H., Choi, J.-H., Nagamine, K. 2011, MNRAS, 412, 411
- Yoshiura, S., Shimabukuro, H., Takahashi, K., Momose, R., Nakanishi, H., Imai, H., 2015, MNRAS, 451, 266
- Zheng, W., Kriss, G. A., Telfer, R. C., Grimes, J. P., Davidsen, A. F. 1997, ApJ, 475, 469

This paper has been typeset from a $\text{\TeX}/\text{\LaTeX}$ file prepared by the author.